文章编号:0253-2778(2018)03-0175-09

Nitrogen-rich a-MEGO@g-C_3N_4 coating on separator for advanced Li-S battery

DU Juan, JIN Song, DU Zhenzhen, JI Hengxing

(*Department of Materials Science and Engineering, CAS Key Laboratory of Materials for Energy Conversion, Collaborative Innovation Center of Chemistry for Energy Materials, University of Science and Technology of China, Hefei 230026, China*)

Abstract: Lithium-sulfur batteries are widely seen as a promising next-generation energy storage system owing to their ultrahigh energy density and environmental benignity, yet the low electrical conductivity of sulfur and the shuttle effect of dissolved polysulfides result in poor cycling performance. An a-MEGO@g-C_3N_4 composite coated on polypropylene separator with high nitrogen content (atomic percent 20.08%) and specific surface area (1000 $m^2 \cdot g^{-1}$) was developed to inhibit polysulfide shuttling. The prepared lithium-sulfur battery with the a-MEGO@g-C_3N_4 coated separator delivered a specific capacity of 1244 mAh $\cdot g^{-1}$ at 0.1C (1C=1675 mA $\cdot g^{-1}$) and a capacity decay rate of 0.062% per cycle after 800 charge/discharge cycles at 0.5 C, which are both superior to the battery assembled with standard separator. Further experimental studies indicate that the improved electrochemical performance is attributed to the superior surface area and nitrogen content which immobilize the polysulfides and reuse the trapped active material. This work is expected to benefit the future development of g-C_3N_4 based carbon materials with optimal nitrogen content and surface area for Li-S batteries.

Key words: separator; g-C_3N_4; chemical adsorption; Li-S battery

CLC number: O646.21; TM911 **Document code**: A doi:10.3969/j.issn.0253-2778.2018.03.001

Citation: DU Juan, JIN Song, DU Zhenzhen, et al. Nitrogen-rich a-MEGO@g-C_3N_4 coating on separator for advanced Li-S battery[J]. Journal of University of Science and Technology of China, 2018,48(3):175-183,198.

杜娟,金松,杜真真,等. 用于高性能锂硫电池隔膜的 a-MEGO@g-C_3N_4 复合材料[J]. 中国科学技术大学学报,2018,48(3):175-183,198.

用于高性能锂硫电池隔膜的 a-MEGO@g-C_3N_4 复合材料

杜 娟,金 松,杜真真,季恒星

(中国科学技术大学材料科学与工程系,中国科学院能量转换材料重点实验室,能源材料化学协同创新中心,安徽合肥 230026)

摘要:由于具有高能量密度和环境友好性,锂硫电池成为备受关注的下一代电化学储能系统,然而硫和硫化锂的低电导率和多硫化锂的穿梭效应严重影响锂硫电池的实际比容量和循环性能.本研究制备出了具有高氮含量(原子数分数 20.08%)和高比表面积(1000 $m^2 \cdot g^{-1}$)的 a-MEGO@g-C_3N_4 复合材料,并将其用作隔膜修饰层.在 0.1C (1C=1675mA $\cdot g^{-1}$)的充放电速度下,采用修饰隔膜的电池首次放电容量达 1244 mAh $\cdot g^{-1}$;

Received: 2017-04-05; **Revised**: 2017-05-15

Foundation item: Supported by the National Natural Science Foundation of China(21373197).

Biography: DU Juan, female, born in 1993, master candidate. Research field: nitrogen-rich carbon-basedmaterials. E-mail: dj2014@mail.ustc.edu.cn

Corresponding author: JI Hengxing, PhD/Prof. E-mail: jihengx@ustc.edu.cn

在0.5 C下循环800次，衰减率为0.062 %，两项指标明显优于对比电池.实验研究发现，a-MEGO@g-C_3N_4隔膜修饰后电池性能的提高来源于两方面：①高比表面积的a-MEGO@g-C_3N_4通过物理吸附固定多硫化物；②g-C_3N_4与多硫化锂通过形成C-S键与Li-N键抑制穿梭效应，并对溶解的活性物质实现再利用.本研究为以g-C_3N_4为基础的高氮碳材料在锂硫电池中的应用提供了可能.

关键词：隔膜；氮化碳；化学吸附；锂硫电池

0 Introduction

Lithium-sulfur (Li-S) batteries have become appealing in the last few years due to their outstanding theoretical capacity of 1675 mAh·g^{-1} and specific energy of 2600 Wh·kg^{-1}[1-4]. However, the low conductivity of sulfur/lithium sulfide and the shuttle effect of polysulfide produced during discharge has long been identified as major problems for developing Li-S batteries[5-6]. To overcome these obstacles, a variety of modifications have been considered, for example, integrating nanostructured carbon materials with sulfur[7-11], modifying the separator surface[12-15], and applying novelty electrolytes[16].

Among these tremendous works to circumvent the dissolution of polysulfides, modifying the separator is a straightforward method to mitigate the migrating of polysulfides. The modified separator can serve as natural support for the barrier layer of polysulfides to trap and reutilize dissolved polysulfides. However, the reported coating materials on separators are mostly porous carbon and the weak physical interaction between porous carbons with dissolvable lithium polysulfides is unsatisfactory to ensure long-term restriction of polysulfides shuttle effect[14,17-18]. Recent reports have demonstrated that the introduction of nitrogen heteroatoms into separators/cathodes can strengthen the interaction between the polysulfides species and the nitrogen anchoring sites by creating a functional polysulfide-trapping interface[19-23]. Thus, seeking for a material with higher nitrogen concentrations may provide more active sites to restrain the diffusion of polysulfide. However, most of the reported nitrogen-doped carbon materials for Li-S batteries have a low nitrogen content (mass fraction less than 10%)[19-20,24-25]. Graphitic-carbon nitride (g-C_3N_4), a light-weight polar host material with a structure analogous to layered graphite has a high nitrogen content (theoretically up to mass fraction 60%).[26] Additionally, g-C_3N_4 can accommodate the volume expansion upon formation of Li_2S on discharge due to its structural elasticity[26]. However, the low electrical conductivity of g-C_3N_4 may result in fast capacity decay on cycling.

Herein, we synthesized a high N-content (atomic percent 20.08%) a-MEGO@g-C_3N_4 composite and reported a feasible modification of the commercial polypropylene (PP) separator with a thin layer of a-MEGO@g-C_3N_4 to suppress the migration of soluble polysulfides. The a-MEGO@g-C_3N_4 coating layer is 0.2 mg·cm^{-2} (the weight of the PP separator is 1.3 mg·cm^{-2}), which overcomes the drawbacks of the added significant weight of the free-standing components employed in previous works. The Li-S battery assembled with a-MEGO@g-C_3N_4 modified separator possesses an initial capacity of 1244 mAh·g^{-1} at 0.1C (1C=1675mA·g^{-1}) and a low capacity fading rate of 0.062% per cycle over 800 cycles at 0.5C. An in-depth study indicates that the high surface area and high nitrogen contents of a-MEGO@g-C_3N_4 can suppress the migration of polysulfides not only via the physical adsorption but also the strong chemical interaction between the nitrogen anchoring sites and polysulfides, which allows a large portion of polysulfide to be captured for further utilization.

1 Experimental

1.1 Synthesis of a-MEGO@g-C_3N_4 composite

a-MEGO was synthesized according to Zhu's

work[27]. a-MEGO @ g-C_3N_4 was produced by heating a-MEGO and melamine in their mixed methanol dispersions. Typically, melamine and a-MEGO methanol dispersion with a weight ratio of 1∶1 were mixed by stirring for 30min first and then heated at 50℃. Once the solvent was removed, the dried product was ball-milled at 500r/min for 10h through ball grinder. And then, the ball-milled mixture was placed into a crucible with a cover and first heated to 340℃ by 10℃ · min^{-1}, then 1℃ · min^{-1} to 380℃ and held for 10 min, and finally the sample was heated by 10℃ · min^{-1} to 550℃ for 7h. All the heating procedures were under the protection of Ar atmosphere. Finally, the sample was allowed to cool to room temperature and labelled as a-MEGO@g-C_3N_4.

1.2 Preparation of the pure sulfur cathode

For the fabrication of sulfur electrodes, a well-mixed sulfur slurry (60% mass fraction of sulfur as active material, 30% mass fraction of Ketjen Black as conductive agent and 10% mass fraction of binder) was coated onto an aluminum foil current collector by doctor blading. The elastomeric binder was a mixture of SBR (styrene-butadiene rubber) and CMC (carboxymethylcellulose sodium) in an empirically optimized weight ratio of 1∶1. For non-modified separator cells, we used cathodes with S∶carbon black∶(CMC+SBR)=50%∶40%∶10%(mass fraction) in order to keep similar sulfur/carbon ratios. The obtained cathodes were punched into circular disks of 10mm after drying in an oven at 50 ℃ for 20 h. The areal sulfur loading on the cathode was approximately 0.8～1 mg · cm^{-2} for the main electrochemical tests.

1.3 Preparation of the coated separator

A simple modification of the PP separator was conducted by directing coating of a-MEGO @ g-C_3N_4 slurry on one side of the separator using a doctor blade method. The slurry was prepared by mixing a-MEGO@g-C_3N_4 (mass fraction 90%) and polyvinyl difluoride (PVDF) (mass fraction 10%) in N-methyl-2-pyrolidone (NMP) solvent. The modified separator was punched into circular disks of 16mm after drying in an oven at 45 ℃ for 20 h. The mass of the coatings was 0.2 mg · cm^{-2}. For comparison, a-MEGO modified separator was produced with a-MEGO slurry by the same method.

1.4 Electrochemical measurements

Common 2032-type coin batteries were assembled in an Ar-filled glovebox with the modified separator and PP separator inserted between cathode and Li metal. The modified separator was placed into the cell with the coating layer facing the cathode. A mixture of 1.0 mol/L lithium bis(trifluoromethanesulfonyl)imide in 1,3-dioxolane and 1, 2-dimethoxyethane (1∶1 by volume) with 2% (mass fraction) $LiNO_3$ additive was used as electrolyte.

The cells were operated in the potential range of 1.7～2.8 V versus Li/Li^+ using a CT2001A battery test system (LAND Electronic Co.). The electrochemical impedance spectroscopy (EIS) tests were carried out between 100 kHz and 10 mHz with an AC voltage amplitude 5mV at the open-circuit voltage of the cells by PARSTAT4000. For the long term cycling tests at 0.5 C, the cells were cycled at 0.1 C for the first two cycles as a preconditioning step.

1.5 Characterization

The morphology of the samples were characterized using a JSM-2100F (JEOL Ltd.) operated at 5.0 kV. Energy-dispersive X-ray spectrometry (EDXS) measurements were taken on the SEM with an EDXS spectrometer. XRD patterns were performed using a D/max-TTR Ⅲ with Cu Kα radiation of λ=1.54178 Å operating at 40 kV and 200 mA. Nitrogen adsorption experiments were conducted using a Quantachrome Autosorb-IQ instrument. EA (elemental analysis) was performed on a Vario EL cube (Elementar Analysensysteme GmbH). X-ray photoelectron spectroscopy (XPS) analysis was conducted with a Thermo ESCALAB 250 instrument using a magnesium anode (monochromatic Kα X-rays at

1486.6 eV) as the source. All spectra were calibrated using the C 1s level (284.8 eV corresponding to C-C) as reference. The cycled separators were washed with DOL/DME solvent inside the glove box prior to the SEM/EDXS and XPS investigations.

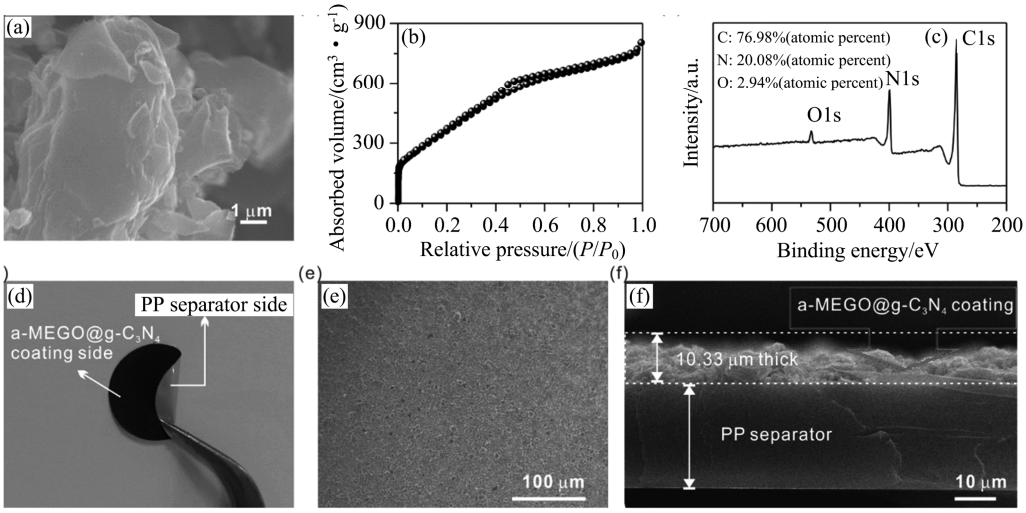

(a) SEM image of synthesized a-MEGO@g-C_3N_4. (b) N_2 adsorption/desorption isotherm of a-MEGO@g-C_3N_4. (c) XPS survey spectrum of a-MEGO@g-C_3N_4. (d) Digital image of as-prepared a-MEGO@g-C_3N_4 coating separator. (e) Top view and (f) cross-sectional SEM images of a-MEGO@g-C_3N_4 coating separator.

Fig.1 The morphology of a-MEGO@g-C_3N_4

2 Results and discussion

The a-MEGO@g-C_3N_4 composite was synthesized by in situ polycondensation of a-MEGO and melamine. The X-ray photoelectron spectrum (Fig.2(a)) shows the peak at 398.8 eV splits to form an obvious new shoulder peak at 397.8 eV, which is caused by the strong interaction between the a-MEGO and the nitrogen atoms in the g-C_3N_4, indicating a-MEGO and g-C_3N_4 are covalently bonded[28]. The covalently-interconnected porous a-MEGO @ g-C_3N_4 structure offers a firm and conductive framework which can provide an electron pathway for improving active material utilization. The synthesized a-MEGO@g-C_3N_4 presents a layered structure as shown in Fig.1(a). Furthermore, the a-MEGO @ g-C_3N_4 possesses a high specific surface area of 1000 $m^2 \cdot g^{-1}$ (Fig.1(b)). The nitrogen content of the a-MEGO @ g-C_3N_4 can be calculated from the XPS results and measured by the elemental analysis, which show a high content of 20.08% and 19.88% (atomic percent), respectively (Fig.1(c) and Tab.1). This value is much larger than that of other commonly used nitrogen-doping methods such as the NH_3 annealing of porous carbons at elevated temperatures[21, 25, 29]. Based on a sketchy calculation, we note that the 20.08% (atomic percent) nitrogen concertation is sufficient to adsorb all the polysulfides of sulfur cathode.

Tab.1 Elemental analysis and XPS analysis of a-MEGO@g-C_3N_4

a-MEGO @ g-C_3N_4	EA(mass fraction)/%				XPS(atomic percent)/%		
	C	N	H	O	C	N	O
	71.8	24.3	0.84	3.08	76.98	20.08	2.940

The a-MEGO@g-C_3N_4 separator was prepared by casting a slurry which contains a-MEGO @ g-C_3N_4 and PVDF ina weight ratio of 90 : 10 onto a PP separator by doctor blade technique. The a-MEGO @ g-C_3N_4 separator exhibited good flexibility and twistability (Fig. 1 (d)). The a-MEGO@g-C_3N_4 coating exhibited a uniformly distributed dense layer with no evidence of cracks on the surface (Fig.1(e)). The weight of the a-MEGO@g-C_3N_4 film was 0.2mg $\cdot$ cm^{-2}, which accounted for only ~ 13% (mass fraction) of the whole separator. The SEM image taken from the cross-section of the a-MEGO @ g-C_3N_4 separator shows that the thickness of the a-MEGO@g-C_3N_4 film was nearly 10 μm (Fig.1(f).

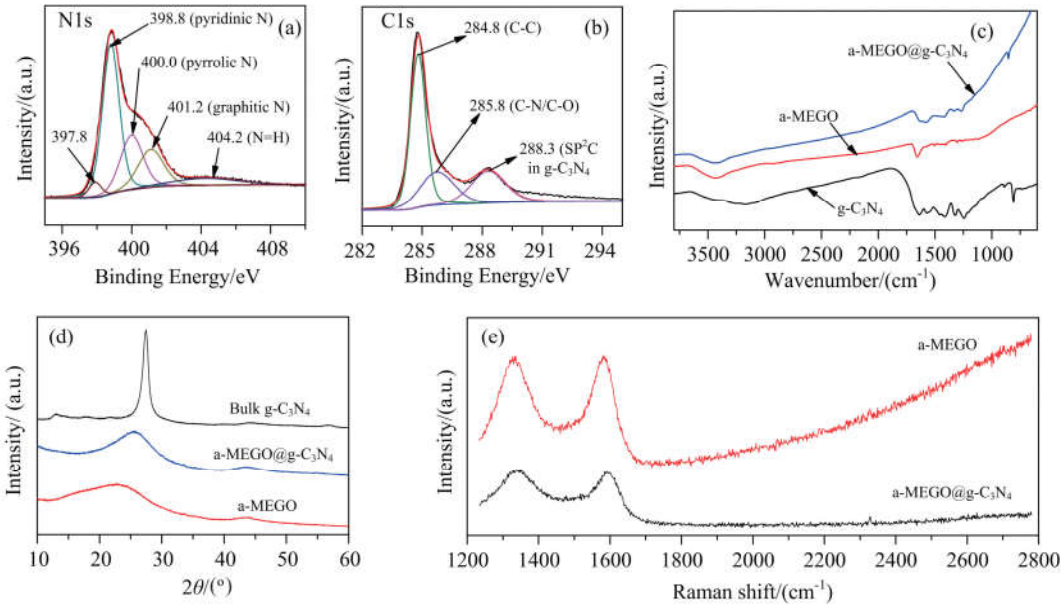

(a, b) N 1s spectrum and C 1s spectrum of a-MEGO@g-C_3N_4, respectively. (c, d) FT-IR spectrums and XRD patterns of the original g-C_3N_4, pristine a-MEGO, a-MEGO@g-C_3N_4, respectively. (e) Raman spectrums of a-MEGO and a-MEGO@g-C_3N_4.

Fig.2　The spectrums of a-MEGO@g-C_3N_4

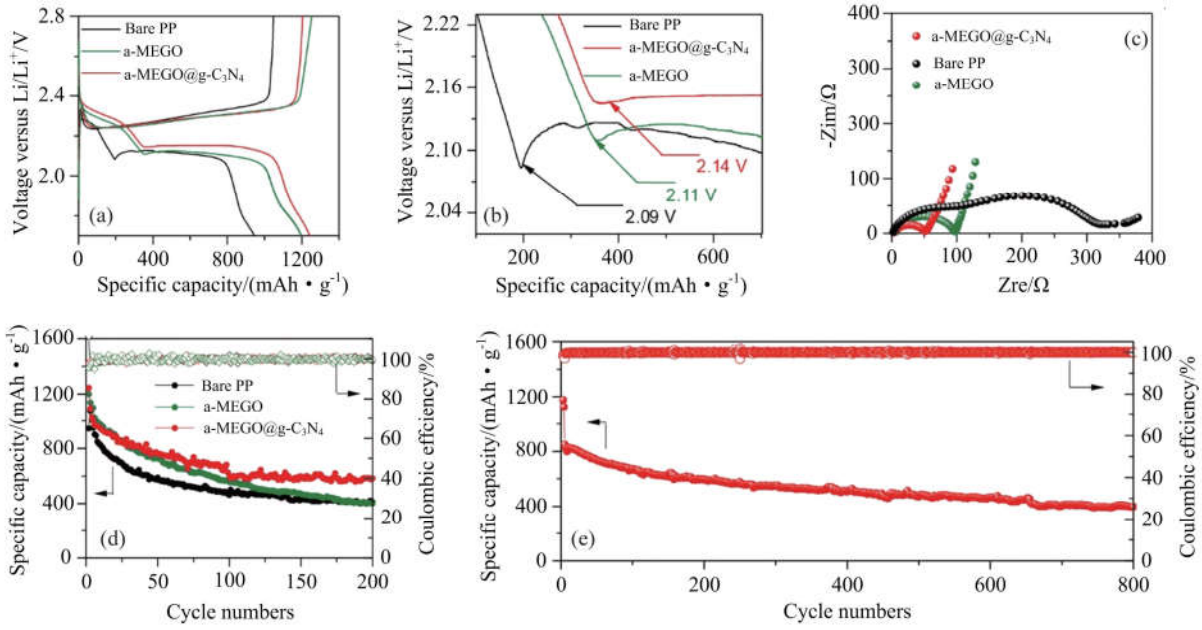

(a) Discharge/charge profiles of Li-S batteries assembled with different types of separators at 0.1 C(1 C=1675 mA • g^{-1}). (b) Discharge profiles of the initial cycle of the Li-S cells assembled with different types of separators. The figure is rescaled to present the beginning of the second discharge plateau. (c) Nyquist plots of Li-S cells assembled with different separators. (d) Discharge capacity and Coulombic efficiency measured at 0.1 C of Li-S cells assembled with different types of separators. (e) Cyclic performance of Li-S cell assembled with a-MEGO@g-C_3N_4 coated separator measured at 0.5 C.

Fig.3　Electrochemical performance of the Li-S cells with different types of separators

The electrochemical performance of the a-MEGO@g-C_3N_4 separator was evaluated in a half-cell with a 1 mol/L LiTFSI in DOL/DME electrolyte and a lithium foil as the counter/reference electrode. Fig. 3(a) shows the charge/discharge profiles of the Li-S batteries assembled with bare PP, a-MEGO separator and a-MEGO@g-C_3N_4 separator, measured at 0.1 C in the voltage

range of 1.7 to 2.8 V versus Li/Li^+. The a-MEGO and a-MEGO @ g-C_3N_4 coating side faced the cathode side when assembling the cell. The Li-S battery assembled with a-MEGO@g-C_3N_4 coating separator could deliver a specific capacity of 1244 mAh·g^{-1} (with respect to the mass of S, both here and below) at 0.1 C, which is 132% and 103% higher than the battery with a standard PP separator and a-MEGO coating separator(Fig. 3(a) and Tab.2).The long-chain polysulfides underwent a nucleation reaction and were converted to non-soluble Li_2S_2 and Li_2S ($Li_2S_4 \leftrightarrow Li_2S$) in the potential range of 2.1～1.7 V.The plateaus of the cells assembled with a-MEGO@g-C_3N_4 separator are longer than the plateaus of the cells with bare PP and a-MEGO coating separator, and the polarization (ΔE) of the cell with a-MEGO@g-C_3N_4 is 120mV, while the ΔE of the cell with a-MEGO and PP separator is 136 mV and 144mV, respectively, showing a significant kinetic advantage to the conversion of soluble Li_2S_4 to insoluble Li_2S (Fig.3(a)).Furthermore, the Li-S cells with a-MEGO @ g-C_3N_4 coating separator exhibit no voltage dip at the beginning of the Li_2S precipitation voltage plateau, which demonstrates the suppressed polysulfide diffusion into the electrolyte (Fig.3(b))[30-31]. The EIS measurements performed on the a-MEGO@g-C_3N_4 coating separator show that the charge transfer resistances is 48.3 Ω, which is much lower than those of the a-MEGO coating separator (92.9 Ω) and bare-PP (245.4 Ω)(see Fig. 4 for details).The battery with a-MEGO@g-C_3N_4 exhibited excellent rate capability as shown in Fig.5. The cell with a-MEGO @ g-C_3N_4 coating separator delivered a specific capacity of 1244 mAh·g^{-1} and 582 mAh·g^{-1} at the 1st and the 200th cycle, respectively (Fig.3(d)). This is a considerable improvement over the cell containing a-MEGO coating separator and bare PP. The long-term cycling stability of a-MEGO@g-C_3N_4 separator was also evaluated (Fig. 3(e)), and after over 800 cycles at 0.5 C, the capacity remained at 398.2 mAh·g^{-1}, corresponding to a capacity retention of 47% of its initial value. The average decay rate of the specific capacity was 0.062 % per cycle, and the Coulombic efficiency at the 800th cycle was 99.89 %.

Tab.2 Electrochemical analysis of Li-S batteries with different separators during 200 cycles at 0.1 C

Separator	Initial discharge capacity (sulfur utilization)/(mAh·g^{-1})	Coulombic efficiency (average in last 50 cycles)/%	Capacity fade rate per cycle/%
a-MEGO@g-C_3N_4 coating	1 244	99.93	0.25
a-MEGO coating	1 198	99.75	0.32
Bare PP	944.0	99.69	0.31

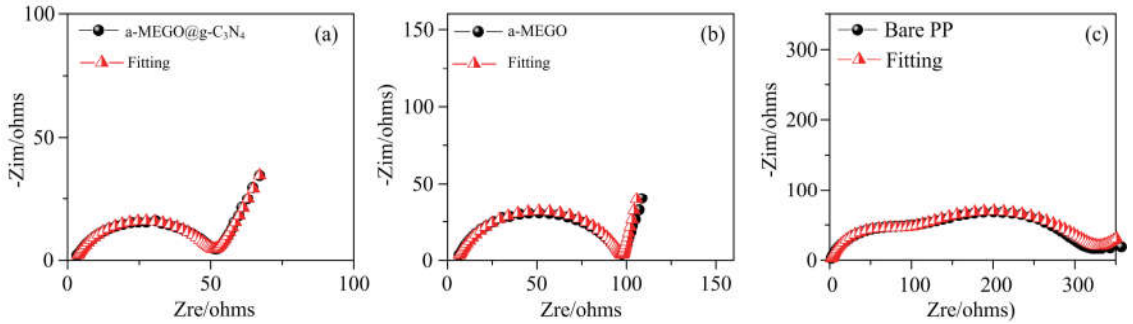

Fig.4 Electrochemical impedance spectroscopy (EIS) plots of the cells with different separators

To study the effect of a-MEGO@g-C_3N_4 coated separator on the electrochemical performance of Li-S batteries, a series of permeation experiments were conducted by using H-shaped devices which were being separated by a-MEGO@g-C_3N_4 separator/ a-MEGO separator and bare PP in order to test

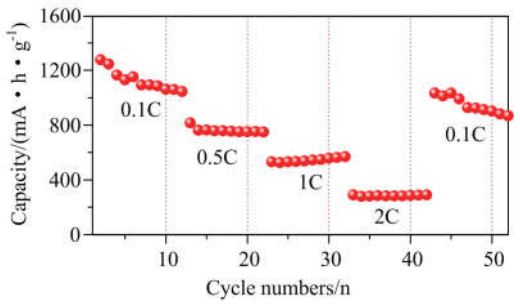

Fig.5　Rate capabilities of the Li-S cell with a-MEGO@g-C_3N_4 coating separator

whether a-MEGO@g-C_3N_4 separator can successfully reduce the diffusion of soluble polysulfides(Fig. 6(a)). The tubes on the left-hand side (L tubes) contained 0.2 mol/L Li_2S_4 dissolved in DOL/DME (1∶1 by volume), while the tubes on the right hand side (R-tubes) contained only DOL/DME solvent. With time increasing, the bare PP separator showed fast diffusion of polysulfides, and the right tube turned dark yellow after 24 h, while the a-MEGO @ g-C_3N_4 separator and a-MEGO separator remained clear with no detectable color change, demonstrating obvious blocking effects towards polysulfides. Although the color of L tube with a-MEGO coating separator and a-MEGO @ g-C3N4 coating separator exhibit no difference to the naked-eye, the UV-Vis spectra of the electrolyte shows that the concentration of the soluble polysulfide released from the a-MEGO separator is 2.5 times of that released from the a-MEGO@g-C_3N_4 separator (Fig.7). After permeation, all separators were analyzed by XPS. The Li 1s spectrum of a-MEGO @ g-C_3N_4/Li_2S_4 shows an asymmetric peak extending to higher binding energy (55.6 eV) and an additional peak at 56.4 eV (Li-N) compared to pristine Li_2S_4 (55.4 eV), which is a result of the Li^+ ions interacting with N[21]. The S 2p spectrum of a-MEGO@g-C_3N_4/Li_2S_4 has a C-S bond at 162.2eV, which is ascribed to the interaction between g-C_3N_4 and Li_2S_4.[32] However, C-S bond is absent in a-MEGO/Li_2S_4 (Fig. 6(e)). These features of XPS demonstrate that polysulfides can be blocked by forming Li-N bond and C-S bond onto a-MEGO @ g-C_3N_4. Moreover, the interaction between polysulfides and a-MEGO @ g-C_3N_4 is further confirmed by FTIR spectra(Fig.8).

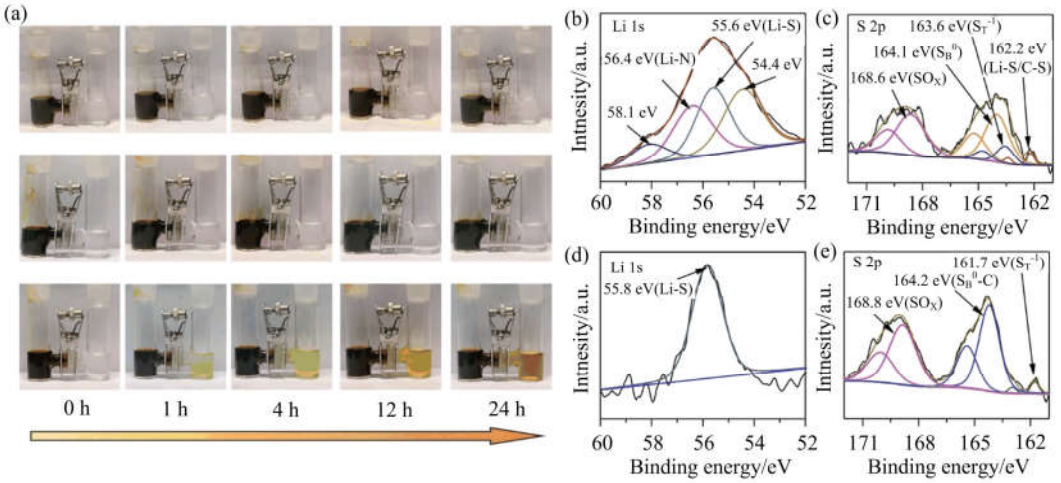

(a)Photograph of H-type cells assembled with a-MEGO@g-C_3N_4 coated separator (upper), a-MEGO coated separator (middle), and bare PP separator (bottom) used for testing the polysulfide permeation. (b,c)XPS Li 1s and S 2p spectra of a-MEGO@g-C_3N_4 coated separator and (d, e) a-MEGO coated separator after the polysulfide permeation measurements.

Fig.6　The effect of a-MEGO@g-C_3N_4 coated separator on minimizing the diffusion of soluble polysulfides

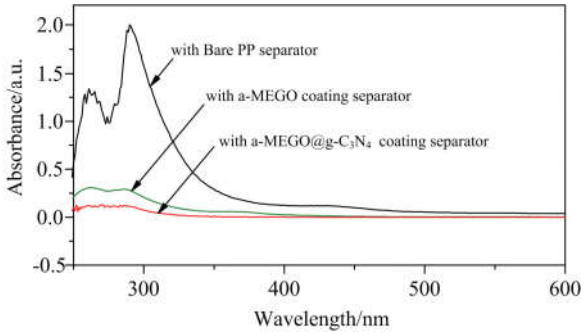

Fig.7 The corresponding UV/Vis spectra of the electrolyte in the R-tube with different separators after keeping the cells still for 24 h

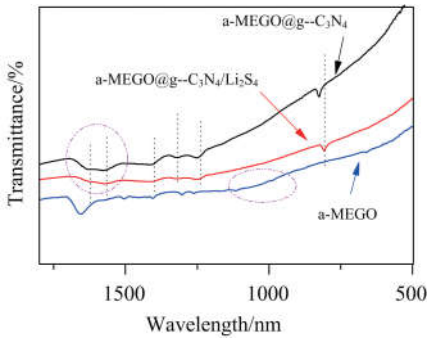

Fig.8 FTIR spectrum of a-MEGO@g-C_3N_4, a-MEGO and a-MEGO@g-C_3N_4/Li_2S_4, respectively

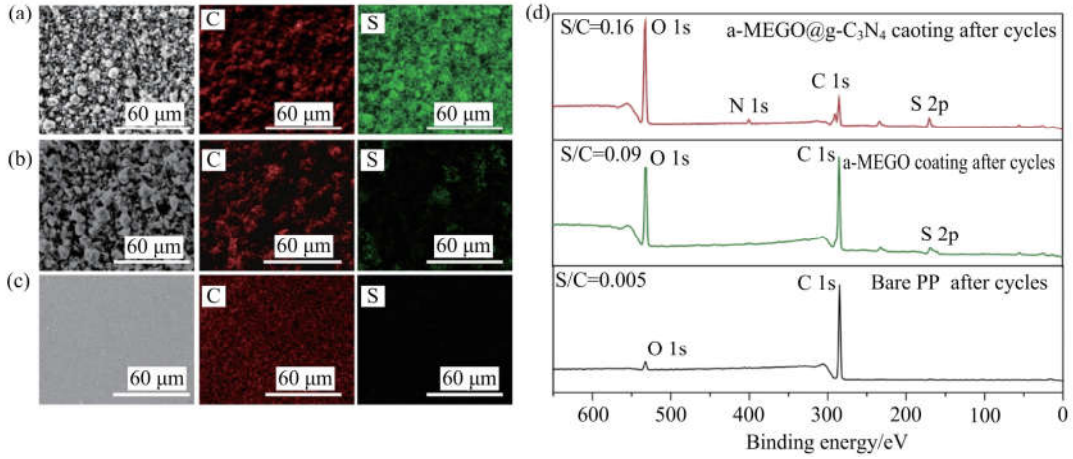

(a,b,c)SEM images and elemental mappings and (d) XPS survey of a-MEGO@g-C_3N_4 coated separator, a-MEGO coated separator, and bare PP separator after cycling.

Fig.9 SEM and XPS characterization of different separators after cycling

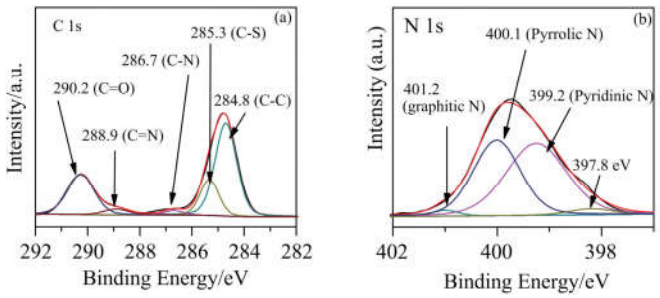

Fig.10 High resolution of C 1s and N 1s XPS of a-MEGO@g-C_3N_4 separator after 100 cycles

To further understand the function of the a-MEGO@g-C_3N_4 coating separator, we disassembled batteries after 100 cycles in a glovebox. The EDS (energy dispersive spectrometer) elemental maps (Fig.9(a)) show a uniform distribution of sulfur in the a-MEGO @ g-C_3N_4 coating separator. S/C atomic ratio from XPS of a-MEGO @ g-C_3N_4 coating separator are 1.8 and 32 times the values of a-MEGO coating separator and bare PP separator, respectively, confirming the effective interception of the dissolved polysulfides with a-MEGO @ g-C_3N_4 coating separator. The C 1s spectrum of a-MEGO@g-C_3N_4 coating separator shows the C—N (285.8 eV) shifts to a slightly higher binding energy (286.7 eV) due to the polarization of the electron away from C atom to electropositive Li of Li_2S (Fig.10), which suggests the strong chemical interaction between g-C_3N_4 and Li_2S[33].

3 Conclusion

In summary, we have designed a separator by coating a-MEGO @ g-C_3N_4 onto a commercial polypropylene separator. The battery with the a-MEGO@ g-C_3N_4 coated separator delivers a high capacity of 1244 mAh·g^{-1} at 0.1C with a capacity fading rate of 0.067% per cycle for 800 cycles at 0.5 C. The improved electrochemical performance of a-MEGO@g-C_3N_4 coating separator attributes to the g-C_3N_4 polarized surface which creates a functional polysulfide-trapping interface by forming C-Sbond and Li-N bond, and the high surface area of a-MEGO@g-C_3N_4 provides abundant physical adsorption sites and serves as a conductive interface during electrochemical cycling.

References

[1] SCROSATI B, HASSOUN J, SUN Y K. Lithium-ion batteries. A look into the future [J]. Energy & Environmental Science, 2011, 4 (9): 3287-3295.

[2] JI X, NAZAR L F. Advances in Li-S batteries [J]. Journal of Materials Chemistry, 2010, 20 (44): 9821.

[3] YIN Y X, XIN S, GUO Y G, et al. Lithium-sulfur batteries: Electrochemistry, materials, and prospects [J]. Angewandte Chemie International Edition, 2013, 52 (50): 13186-13200.

[4] ZHOU G, PEI S, LI L, et al. A graphene-pure-sulfur sandwich structure for ultrafast, long-life lithium-sulfur batteries [J]. Advanced Materials, 2014, 26 (4): 625-631.

[5] MANTHIRAM A, FU Y, SU Y S. Challenges and prospects of lithium-sulfur batteries [J]. Accounts of Chemical Research, 2012, 46 (5): 1125-1134.

[6] YANG Y, ZHENG G, CUI Y. Nanostructured sulfur cathodes [J]. Chemical Society Reviews, 2013, 42 (7): 3018-3032.

[7] ZHOU G, WANG D W, LI F, et al. A flexible nanostructured sulphur-carbon nanotube cathode with high rate performance for Li-S batteries [J]. Energy & Environmental Science, 2012, 5 (10): 8901-8906.

[8] ZHOU G, LI L, MA C, et al. A graphene foam electrode with high sulfur loading for flexible and high energy Li-S batteries [J]. Nano Energy, 2015, 11: 356-365.

[9] LI G, SUN J, HOU W, et al. Three-dimensional porous carbon composites containing high sulfur nanoparticle content for high-performance lithium-sulfur batteries [J]. Nature Communications, 2016, 7: 10601-10611.

[10] JI X, EVERS S, BLACK R, et al. Stabilizing lithium-sulphur cathodes using polysulphide reservoirs [J]. Nature Communications, 2011, 2: 325-332.

[11] WANG D W, ZENG Q, ZHOU G, et al. Carbon-sulfur composites for Li-S batteries: Status and prospects [J]. Journal of Materials Chemistry A, 2013, 1 (33): 9382-9394.

[12] BAI S, LIU X, ZHU K, et al. Metal-organic framework-based separator for lithium-sulfur batteries [J]. Nature Energy, 2016, 1: 16094-16100.

[13] HUANG J Q, ZHANG Q, PENG H J, et al. Ionic shield for polysulfides towards highly-stable lithium-sulfur batteries [J]. Energy & Environmental Science, 2014, 7 (1): 347-353.

[14] YAO H, YAN K, LI W, et al. Improved lithium-sulfur batteries with a conductive coating on the separator to prevent the accumulation of inactive S-related species at the cathode-separator interface [J]. Energy & Environmental Science, 2014, 7 (10): 3381-3390.

[15] CHUNG S H, HAN P, SINGHAL R, et al. Electrochemically stable rechargeable lithium-sulfur batteries with a microporous carbon nanofiber filter for polysulfide [J]. Advanced Energy Materials, 2015, 5 (18): 1500738-1500750.

[16] ZHANG S, UENO K, DOKKO K, et al. Recent advances in electrolytes for lithium-sulfur batteries [J]. Advanced Energy Materials, 2015, 5 (16): 1500117-1500145.

[17] BALACH J, JAUMANN T, KLOSE M, et al. Functional mesoporous carbon-coated separator for long-life, high-energy lithium-sulfur batteries [J]. Advanced Functional Materials, 2015, 25 (33): 5285-5291.

[18] ZHU J, GE Y, KIM D, et al. A novel separator coated by carbon for achieving exceptional high performance lithium-sulfur batteries [J]. Nano Energy, 2016, 20: 176-184.

[19] BALACH J, JAUMANN T, KLOSE M, et al. Improved cycling stability of lithium-sulfur batteries using a polypropylene-supported nitrogen-doped mesoporous carbon hybrid separator as polysulfide adsorbent [J]. Journal of Power Sources, 2016, 303: 317-324.

[20] ZHANG Z, WANG G, LAI Y, et al. Nitrogen-doped porous hollow carbon sphere-decorated separators for advanced lithium-sulfur batteries [J]. Journal of Power Sources, 2015, 300: 157-163.

(下转第 198 页)